JACS
JOURNAL OF THE AMERICAN CHEMICAL SOCIETY
Communication
pubs.acs.org/JACS

Grain-Boundary-Dependent CO_2 Electroreduction Activity

Xiaofeng Feng,[†] Kaili Jiang,[‡] Shoushan Fan,[‡] and Matthew W. Kanan*,[†]

[†]Department of Chemistry, Stanford University, 337 Campus Drive, Stanford, California 94305, United States
[‡]Department of Physics and Tsinghua-Foxconn Nanotechnology Research Center, Tsinghua University, Beijing 100084, China

Supporting Information

ABSTRACT: Uncovering new structure−activity relationships for metal nanoparticle (NP) electrocatalysts is crucial for advancing many energy conversion technologies. Grain boundaries (GBs) could be used to stabilize unique active surfaces, but a quantitative correlation between GBs and catalytic activity has not been established. Here we use vapor deposition to prepare Au NPs on carbon nanotubes (Au/CNT). As deposited, the Au NPs have a relatively high density of GBs that are readily imaged by transmission electron microscopy (TEM); thermal annealing lowers the density in a controlled manner. We show that the surface-area-normalized activity for CO_2 reduction is linearly correlated with GB surface density on Au/CNT, demonstrating that GB engineering is a powerful approach to improving the catalytic activity of metal NPs.

Metal nanoparticles (NPs) comprise a large portion of the electrocatalysts utilized for energy conversion reactions. Most efforts to tailor NP surfaces have focused on controlling particle size, shape, and composition.[1−4] Although this approach enables systematic structural changes, it is unclear if its accessible structure space is sufficient for finding optimal catalysts. Moreover, NPs often change their morphology and composition during electrocatalysis.[5] A possible alternative is to use bulk defects such as GBs to stabilize catalytically active surfaces.[6−8] Bulk defects may support active surface structures under catalysis conditions that would otherwise be unstable. Here we provide evidence that GBs engender high activity for CO_2 reduction to CO catalyzed by Au NPs.

Numerous recent reports have described Au NP CO_2 reduction catalysts with widely varying current density, mass activity, and Faradaic efficiency (FE).[9−13] A study of size effects revealed that very small Au NPs are poor CO_2 reduction catalysts because their high coverage of surface corner sites strongly favors H^+ reduction.[11] Ultrathin Au nanowires were shown to have high FE for CO_2 reduction to CO at low overpotentials, which suggests that edge sites are particularly active.[12] However, a quantitative correlation between the surface coverage of a particular structural feature and the surface-area-normalized activity for CO_2 reduction has not been described for Au NPs, making it difficult to interpret differences in activity or FE.

We recently showed that the reduction of Cu oxide and Au oxide films results in metallic catalysts ("oxide-derived" metals) composed of highly interconnected nanocrystals linked by GBs.[8,14−16] Oxide-derived Cu (OD-Cu) has lower specific (i.e., surface-area-normalized) activity for H^+ reduction and enhanced specific activity for CO reduction compared to other Cu materials, and OD-Au has higher specific activity for CO_2 reduction to CO compared to other Au materials. These features result in high selectivity for CO_2 reduction vs H^+ reduction at low overpotential on both OD-Cu[14] and OD-Au[15] and high selectivity for CO reduction to liquid oxygenates on OD-Cu.[8] The high density of GBs in these nanocrystalline thin films suggests that the boundaries may be responsible for their catalytic properties.

Establishing a quantitative correlation between GB density and catalytic activity in OD-metals is challenging because it is difficult to modulate the density and extensive processing is required to prepare samples for TEM. We hypothesized that GB-rich NPs prepared by metal vapor deposition could recapitulate the catalytic properties of OD-metals and facilitate the study of GB−activity relationships. Carbon nanotubes (CNTs) were chosen as the substrate because of their high conductivity, high stability, and low background activity.

Au/CNT electrodes were prepared by using e-beam evaporation to deposit Au at a rate of 2 Å s^{-1} for 50 s on a CNT film that was pulled from a superaligned CNT array (Figure S1).[17−19] Figure 1a shows TEM images of Au/CNT as deposited. A large fraction of the CNT surfaces were covered with Au NPs. X-ray photoelectron spectroscopy showed only the expected Au and C peaks (Figure S2). High-resolution TEM images (Figure 1a, right) revealed that many of the NPs were polycrystalline. The particle sizes and GBs were analyzed by imaging ∼300 NPs from as-deposited Au/CNT (Figures S3, S4). The average particle size was 18.3 ± 4.4 nm, and each particle had between 0 and 4 GBs that were readily visible in the TEM image. These metrics are consistent with Williamson−Hall analysis of the grazing incidence X-ray diffraction pattern, which indicated an average Au crystallite size of 11 nm (Figure S5). The projected GB length(s) and particle area were measured for each NP image and converted to GB surface lengths (i.e., the length of the GB surface termination) and 3D particle surface areas using simple geometrical models. The fraction of the Au NP surfaces that corresponds to GB surface terminations (hereafter referred to as the "GB surface density") was calculated by dividing the sum of all of the GB surface lengths by the sum of the NP surface areas (see Supporting Information). The GB surface density was 49.5 μm^{-1} for the as-deposited sample (Table 1).

To change the microstructure of the vapor-deposited Au NPs, Au/CNT samples were annealed under air at 200, 300,

Received: December 22, 2014
Published: April 2, 2015

DOI: 10.1021/ja5130513
J. Am. Chem. Soc. 2015, 137, 4606−4609

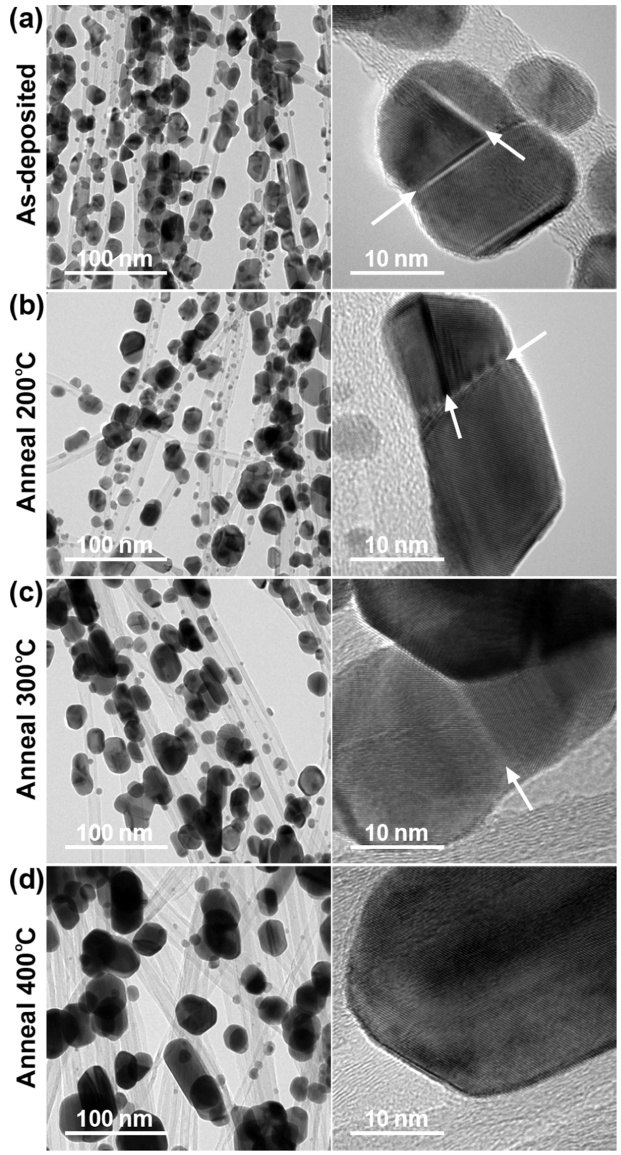

Figure 1. TEM images of as-deposited and annealed Au/CNT electrodes. The left column shows overview images of the four electrodes, and the right shows representative high-resolution TEM images of the Au NPs. The arrows indicate grain boundaries in the NPs.

Table 1. Structural Metrics for Au/CNT Electrodes

sample	NP size (nm)	GB surface density (μm^{-1})	surface area ($cm^2\ mg^{-1}$)
Au/CNT	18.3 ± 4.4	49.5 ± 4.5	92 ± 3
Au/CNT_200	20.8 ± 5.3	28.1 ± 2.4	93 ± 3
Au/CNT_300	26.3 ± 5.6	13.3 ± 1.0	96 ± 4
Au/CNT_400	33.8 ± 7.9	4.2 ± 0.3	56 ± 2

and 400 °C (Au/CNT_200, Au/CNT_300, and Au/CNT_400, respectively). The use of an air atmosphere prevented the formation of carbon coatings on the Au NPs. XPS analysis after annealing indicated no significant oxidation of the Au/CNT surface (Figure S6). TEM images of the annealed samples are shown in Figure 1b–1d. Analysis of ~300 NPs from each sample was performed as described above to characterize the microstructure (Figures S3, S4). As the annealing temperature was increased, the average particle size increased slightly and the GB surface density decreased substantially (Table 1). The Au/CNT_400 sample had a GB surface density of only 4.2 μm^{-1}, over 1 order of magnitude smaller than that of the as-deposited Au/CNT sample. We note that there are likely GBs that are not counted in each of the Au/CNT samples because they are not readily visible in the TEM images. The GB surface densities in Table 1 therefore only indicate the relative densities for comparison of the four samples.

Electrodes were prepared from the Au/CNT films by rolling them into yarns and connecting the yarns to Au wires. The electrochemically accessible Au surface areas of the electrodes were measured using Cu underpotential deposition (upd).[20] As-deposited Au/CNT, Au/CNT_200, and Au/CNT_300 had very similar Au surface areas, while the surface area of Au/CNT_400 was approximately 40% lower (Figure 2a and Table 1). The distribution of Au surface facets was probed using Pb upd.[21−23] All of the electrodes showed only two significant peaks in the Pb upd voltammogram that correspond to the (111) and (110) facets (Figure 2b). Thus, annealing at up to 400 °C has very little effect on the surface area or surface faceting of Au/CNT, enabling their use to interrogate the effect of GB surface density independently of other morphological changes.

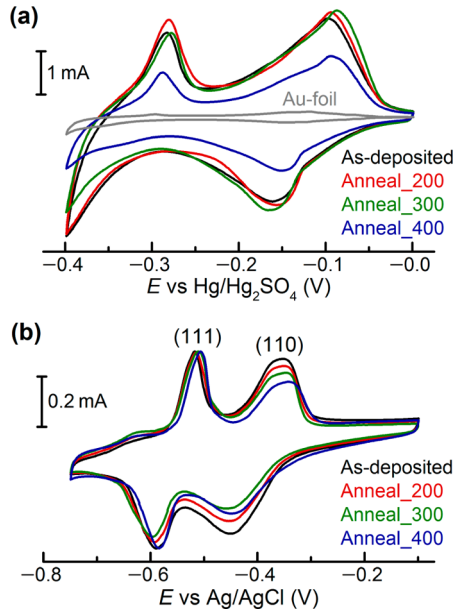

Figure 2. Electrochemical surface characterization. (a) Cu-upd voltammetry of the Au/CNT electrodes (mass ≈ 0.20 mg) and polycrystalline Au foil (1 cm^2). (b) Pb-upd profiles of the Au/CNT electrodes. The profiles were normalized to match the peak heights of the (111) features. Scan rate: 50 mV/s.

The CO_2 reduction activities of the Au/CNT electrodes were measured in a series of constant-potential electrolyses performed in 0.5 M $NaHCO_3$ saturated with 1 atm of CO_2. CO and H_2 were the only significant products observed and were quantified at 15 min intervals using gas chromatography. The product distributions and current densities were stable over multiple hours on all electrodes (see below), which enabled comparison of their steady-state catalytic properties. The current density of the CNT film without Au was <2% of the Au/CNT electrodes.

DOI: 10.1021/ja5130513
J. Am. Chem. Soc. 2015, 137, 4606−4609

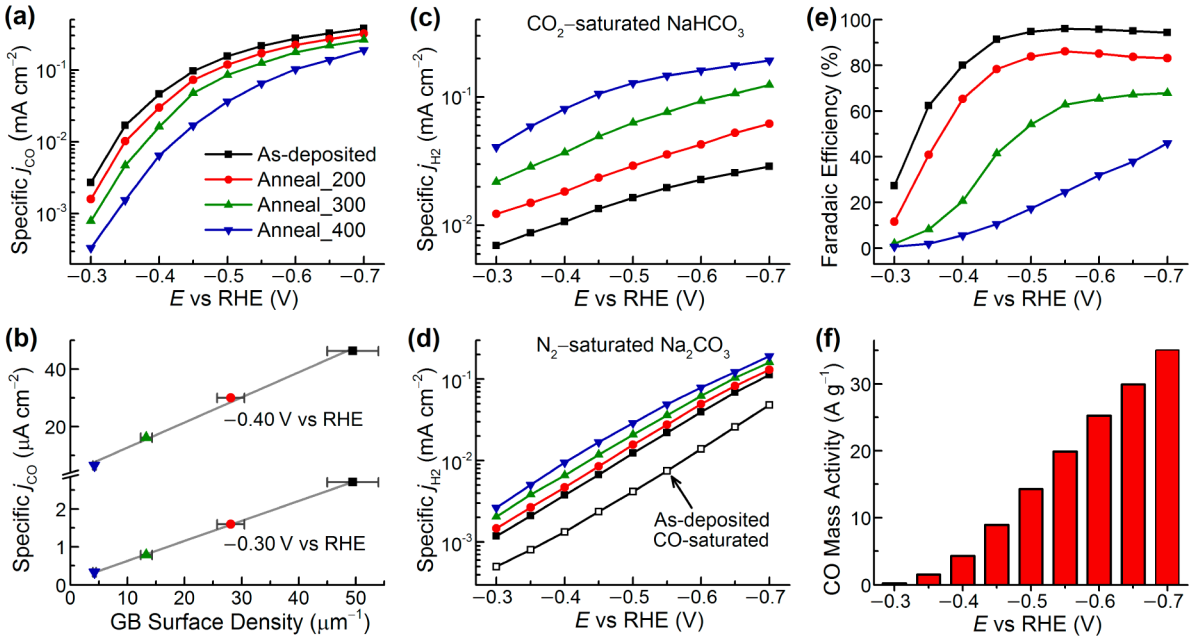

Figure 3. Structure–activity correlation for the Au/CNT electrodes. (a) Specific current density for CO production (j_{CO}) vs potential. (b) Correlation between specific j_{CO} and GB surface density at low overpotentials. (c) Specific current density for H_2 production (j_{H2}) in CO_2-saturated 0.50 M $NaHCO_3$ electrolyte. (d) Specific j_{H_2} in N_2- or CO-saturated 0.25 M Na_2CO_3 electrolyte. (e) Faradaic efficiency for CO production vs potential. (f) Mass activity for CO production on as-deposited Au/CNT electrode.

The Au/CNT electrodes exhibited strikingly different CO_2 reduction activities depending on the annealing pretreatment. The specific current density for CO production (specific j_{CO}) was the highest for as-deposited Au/CNT and decreased as the annealing pretreatment temperature was increased. Figure 3a shows the Tafel plots ($\log(j_{CO})$ vs potential) for each electrode. From −0.3 to −0.4 V, the specific j_{CO} differed by approximately an order of magnitude between the most active (as-deposited) to least active (Au/CNT_400) electrode. At more negative potentials, the Tafel plots plateaued and the differences in specific j_{CO} between the electrodes were compressed.

CO_2 reduction activity was correlated with GB surface density in the Au/CNT electrodes. From −0.3 to −0.4 V, the relationship between the specific j_{CO} and GB surface density was linear across all samples (Figure 3b). Since the electrodes have very similar Au surface areas and surface faceting, this result suggests that the GB surface terminations are responsible for most of the CO_2 reduction activity at low overpotentials while the (111) and (110) facets are relatively inactive. At higher overpotentials (<−0.4 V), the relationship between the specific j_{CO} and GB surface density deviated from linearity as the differences in activity were compressed (Figure S7). This change may be explained by a combination of the increased activity of (111) and (110) facets in the high overpotential regime, saturation of highly active GB-associated sites, and an increased dependence of the kinetics on mass transport effects.

The difference in CO_2 reduction activity was accompanied by a difference in H_2 evolution activity among the Au/CNT electrodes in the CO_2-saturated electrolyte. At all potentials examined, the specific current density for H_2 evolution (specific j_{H_2}) was the lowest for the as-deposited sample and increased as the annealing pretreatment temperature was increased (Figure 3c). The range of specific j_{H_2} spanned a factor of 6 between highest (Au/CNT_400) and lowest (as-deposited Au/CNT). When evaluated in N_2-saturated 0.25 M Na_2CO_3, however, the range was much smaller, spanning approximately a factor of 2 (Figure 3d). Moreover, bubbling CO through the Na_2CO_3 electrolyte caused an approximately 3-fold reduction in j_{H_2} (Figure 3d), while bubbling CO through electrolyses in CO_2-saturated $NaHCO_3$ caused a 2-fold reduction (Figure S8). Together, these experiments indicate that the difference in specific j_{H_2} between the Au/CNT electrodes in the CO_2-saturated HCO_3^- electrolyte is largely a consequence of the difference in their CO_2 reduction activities. The higher the activity for CO_2 reduction to CO, the greater the local concentration of CO is near the electrode surface. The CO inhibits H_2 evolution by reversibly binding to the Au surface sites responsible for this reaction.

The differences in CO_2 reduction and H_2 evolution activities between the Au/CNT electrodes translate into large differences in selectivity. Figure 3e shows the FE for CO vs potential. As evident from the j_{CO} and j_{H_2} values, at all potentials the FE for CO was the highest for as-deposited Au/CNT and decreased as the annealing pretreatment temperature was increased. The difference in FE between the most- and least-selective electrodes is striking: the FE for CO on Au/CNT_400 at −0.7 V is lower than the FE on as-deposited Au/CNT at only −0.35 V.

The as-deposited Au/CNT electrodes exhibit high mass activities for CO production that are sustained over prolonged electrolyses. The quasi steady-state mass activity (amps of CO synthesis per g Au, averaged over 1–2 h) ranged from 0.3 A g^{-1} at −0.3 V to 35 A g^{-1} at −0.7 V (Figure 3f). We note that the mass activities at potentials <−0.4 V may not reflect the true electroreduction activity of Au/CNT because mass transport limitations may significantly suppress j_{CO} in this regime. In an electrolysis lasting 12 h at −0.5 V, the FE for CO remained constant at ∼94% and the mass activity declined slowly from 15 to 13 A g^{-1} (Figure 4a). This decline may reflect a small amount of sintering that occurs during electrolysis. TEM

DOI: 10.1021/ja5130513
J. Am. Chem. Soc. 2015, 137, 4606–4609

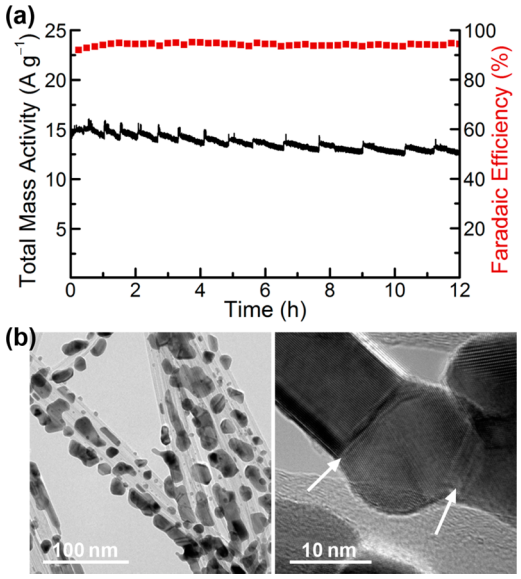

Figure 4. Stability of the as-deposited Au/CNT electrode. (a) Time-dependent total mass activity (black, left-axis) and Faradaic efficiency for CO production (red, right-axis) for electrolysis at −0.50 V vs RHE in CO_2-saturated 0.5 M $NaHCO_3$. The current fluctuations were caused by gas bubble release. (b) Representative TEM images of the electrode after a 12 h electrolysis showing that grain boundaries are retained.

analysis of the electrode after 12 h of electrolysis indicated that the Au NPs were still highly polycrystalline (Figures 4b and S9). The GBs are stable during electrolysis, maintaining high j_{CO} and FE for CO.

The GB−activity relationship in Au/CNT electrodes (Figure 3b) supports the notion that GBs account for the CO_2 reduction activity in OD-Au. Compared to as-deposited Au/CNT, OD-Au has higher specific j_{CO} and a more desirable FE vs potential profile.[15] The GB surface density for OD-Au cannot be measured accurately because of its complex morphology. Nonetheless, it is very likely that the GB surface density is considerably higher on OD-Au because it is a continuous film in which all of the nanocrystallites are linked together by GBs. Au/CNT has a much higher mass activity, however, because it does not require a thick oxide precursor. Altering vapor deposition conditions to increase the GB density of Au NPs on CNTs should lead to proportionally higher specific CO_2 reduction activity. Little is known about the structure of GB surface terminations, which is likely to be highly dependent on the angle of misorientation and the GB inclination.[24] Future work will aim to elucidate the relationships between catalytic activity, GB geometry, and GB surface structure.

In summary, we have shown that there is a linear correlation between the GB surface density and specific activity for CO_2 reduction with vapor deposited Au NPs on CNTs. Because the surface areas and surface faceting of the electrodes compared are all similar, this correlation implicates GB surface terminations as highly active sites for CO_2 reduction. Our work motivates future efforts to deliberately incorporate high GB densities into metal NP electrocatalysts.

■ ASSOCIATED CONTENT

Supporting Information

Experimental details and additional characterization data for Au/CNT electrodes. This material is available free of charge via the Internet at http://pubs.acs.org.

■ AUTHOR INFORMATION

Corresponding Author

*mkanan@stanford.edu

Notes

The authors declare no competing financial interest.

■ ACKNOWLEDGMENTS

We thank the Global Climate and Energy Project (106765) and the National Science Foundation (CHE-1266401) for support of this research.

■ REFERENCES

(1) You, H.; Yang, S.; Ding, B.; Yang, H. *Chem. Soc. Rev.* **2013**, *42*, 2880.
(2) Bandarenka, A. S.; Koper, M. T. M. *J. Catal.* **2013**, *308*, 11.
(3) Tian, N.; Zhou, Z. Y.; Sun, S. G. *J. Phys. Chem. C* **2008**, *112*, 19801.
(4) Solla-Gullón, J.; Vidal-Iglesias, F. J.; Feliu, J. M. *Annu. Rep. Prog. Chem., Sect. C* **2011**, *107*, 263.
(5) Manthiram, K.; Surendranath, Y.; Alivisatos, A. P. *J. Am. Chem. Soc.* **2014**, *136*, 7237.
(6) Gavrilov, A. N.; Savinova, E. R.; Simonov, P. A.; Zaikovskii, V. I.; Cherepanova, S. V.; Tsirlina, G. A.; Parmon, V. N. *Phys. Chem. Chem. Phys.* **2007**, *9*, 5476.
(7) Wang, S.; Jiang, S. P.; White, T. J.; Guo, J.; Wang, X. *J. Phys. Chem. C* **2009**, *113*, 18935.
(8) Li, C. W.; Ciston, J.; Kanan, M. W. *Nature* **2014**, *508*, 504.
(9) Kauffman, D. R.; Alfonso, D.; Matranga, C.; Qian, H.; Jin, R. *J. Am. Chem. Soc.* **2012**, *134*, 10237.
(10) Zhu, W.; Michalsky, R.; Metin, O.; Lv, H.; Guo, S.; Wright, C. J.; Sun, X.; Peterson, A. A.; Sun, S. *J. Am. Chem. Soc.* **2013**, *135*, 16833.
(11) Mistry, H.; Reske, R.; Zeng, Z.; Zhao, Z. J.; Greely, J.; Strasser, P.; Cuenya, B. R. *J. Am. Chem. Soc.* **2014**, *136*, 16473.
(12) Zhu, W.; Zhang, Y. J.; Zhang, H.; Lv, H.; Li, Q.; Michalsky, R.; Peterson, A. A.; Sun, S. *J. Am. Chem. Soc.* **2014**, *136*, 16132.
(13) Kim, D.; Resasco, J.; Yu, Y.; Asiri, A. M.; Yang, P. *Nat. Commun.* **2014**, *5*, 4948.
(14) Li, C. W.; Kanan, M. W. *J. Am. Chem. Soc.* **2012**, *134*, 7231.
(15) Chen, Y.; Li, C. W.; Kanan, M. W. *J. Am. Chem. Soc.* **2012**, *134*, 19969.
(16) Min, X.; Chen, Y.; Kanan, M. W. *Phys. Chem. Chem. Phys.* **2014**, *16*, 13601.
(17) Jiang, K.; Li, Q.; Fan, S. *Nature* **2002**, *419*, 801.
(18) Zhang, X.; Jiang, K.; Feng, C.; Liu, P.; Zhang, L.; Kong, J.; Zhang, T.; Li, Q.; Fan, S. *Adv. Mater.* **2006**, *18*, 1505.
(19) Liu, K.; Sun, Y.; Chen, L.; Feng, C.; Feng, X.; Jiang, K.; Zhao, Y.; Fan, S. *Nano Lett.* **2008**, *8*, 700.
(20) Rouya, E.; Cattarin, S.; Reed, M. L.; Kelly, R. G.; Zangari, G. *J. Electrochem. Soc.* **2012**, *159*, K97.
(21) Hamelin, A. *J. Electroanal. Chem.* **1984**, *165*, 167.
(22) Hamelin, A.; Lipkowski, J. *J. Electroanal. Chem.* **1984**, *171*, 317.
(23) Hernández, J.; Solla-Gullón, J.; Herrero, E. *J. Electroanal. Chem.* **2004**, *574*, 185.
(24) Radetic, T.; Lancon, F.; Dahmen, U. *Phys. Rev. Lett.* **2002**, *89*, 085502.

DOI: 10.1021/ja5130513
J. Am. Chem. Soc. 2015, 137, 4606−4609